J Mater Sci (2006) 41:8160–8165
DOI 10.1007/s10853-006-0420-1

Structural properties of electrophoretically deposited europium oxide nanocrystalline thin films

S. V. Mahajan · D. W. Kavich · M. L. Redigolo · J. H. Dickerson

Received: 14 January 2006 / Accepted: 8 May 2006 / Published online: 28 October 2006

Abstract The structural properties of nanocrystalline europium oxide (Eu_2O_3) thin films, produced via electrophoretic deposition (EPD), were investigated. We found that EPD from our Eu_2O_3 nanocrystal solutions yielded both translucent films, with uniform size and distribution of the microstructure, and opaque films, with marked anisotropy to the size and distribution of the constituents of the microstructure. The disparity in the film morphology arose from the initial temperature conditions of the nanocrystal solution. The translucent films, produced from pre-chilled (–25 °C) EPD solutions, were bimodal films, comprised of homogeneous, tightly packed, glassy nanocrystalline films interspersed with micron-sized nanocrystal aggregates. In contrast, the opaque films, produced from room temperature solutions, consisted of an irregularly distributed and shaped microstructure. The evolution of the microstructure was monitored for the chilled samples as a function of film thickness (deposition time) and juxtaposed with the resultant structure of the room temperature film. Optical microscopy and scanning electron microscopy were employed to characterize the films.

S. V. Mahajan
Interdisciplinary Program in Materials Science, Vanderbilt University, Nashville, TN, USA

D. W. Kavich · M. L. Redigolo · J. H. Dickerson (✉)
Department of Physics and Astronomy, Vanderbilt University, Station B #351807, 2301 Vanderbilt Place, Nashville, TN 37235-1807, USA
e-mail: james.h.dickerson@Vanderbilt.Edu

Introduction

Europium oxide (Eu_2O_3), the stable sesquioxide of the Eu^{3+} ion, has been employed extensively a component phosphor in cathode-ray tube displays and as a phosphorescence agent in other light-emitting compounds [1–6]. The optical properties of Eu_2O_3 originate from the Eu^{3+} ion absorption ($4f \rightarrow 4f^7 2p^{-1}$) and the electric dipole ($^5D_J \rightarrow {}^7F_{\Delta J = 2}$) and magnetic dipole ($^5D_J \rightarrow {}^7F_{\Delta J = 0, \pm 1}$) transitions, whose primary fluorescence peak resides at 612 nm [7–10]. These core optical transitions are relatively unaffected by the size or the surface morphology of the materials. Therefore, Eu_2O_3 is an attractive material for use in a variety of device size regimes, from nanoscale to macroscopic. Recent studies have sought to take advantage of the optical properties of europium oxide nanocrystals and other rare-earth-based materials for implementation in nanoscale optical devices, such as biocompatible bioimaging reagents or nanocrystalline light-emitting diodes [11, 12]. Thin films of Eu_2O_3 nanocrystals also could be employed in nanoscale applications, such as fluorescent video displays [13, 14], photoactive coatings [14, 15], optical data storage [15], and even high-κ dielectrics [16, 17].

One attractive way to integrate nanocrystals into nanoscale optical devices is the controlled assembly and deposition of nanocrystals. Of the well-known deposition techniques for nanocrystals, electrophoretic deposition (EPD) provides the most substantial control over the film thickness, the deposition rate, and film composition homogeneity [18–21]. In this study, we investigated the electrophoretic deposition of Eu_2O_3 nanocrystals on metallic electrodes. We produced two types of thin films with markedly

different microstructure, based on the initial temperature conditions of the nanocrystal solution. Translucent films, created from chilled nanocrystal solutions, were comprised of smooth, homogeneous, transparent, glassy films [22–24] of tightly packed Eu_2O_3 nanocrystals, interspersed with micron-sized (1–5 μm), glassy aggregates of Eu_2O_3 nanocrystals. These micron-sized aggregates also appeared transparent under high optical magnification. However, the size of the aggregates caused the total film to appear hazy due to Mie scattering. In contrast, the opaque films, created from room temperature nanocrystal solutions, consisted of glassy Eu_2O_3 nanocrystal films and micron-sized agglomerates, which were significantly larger, more irregularly shaped, and more unevenly distributed than the chilled solution films. Further, we observed that the film morphology, from the chilled solutions, evolved as a function of the deposition time. To track the differences in the films, we probed their composition and morphology using optical microscopy, scanning electron microscopy (SEM), energy dispersive X-ray spectroscopy (EDS), and photoluminescence spectroscopy (PL).

Experiment

Nanocrystal synthesis

Our approach to synthesize the Eu_2O_3 nanocrystals was adapted from the room temperature colloidal chemistry of Wakefield et al. [10]. The precursor chemicals for the nanomaterials synthesis, Europium (III) chloride hexahydrate ($EuCl_3 \cdot 6H_2O$, 99.99%), Trioctylphosphine oxide (TOPO, $[CH_3(CH_2)_7]_3PO$, 99%), and sodium hydroxide (NaOH, 98%), were obtained from Sigma–Aldrich and were used without further purification. A mixture of methanolic solutions TOPO (5 mM) and $EuCl_3 \cdot 6H_2O$ (5 mM) was prepared in a 1:1 volumetric ratio to synthesize 4.0 nm nanocrystals, with a size distribution of less than 15%. The addition of 50 mM methanolic sodium hydroxide solution to the aforementioned solution initiated the formation of the Eu_2O_3 nanocrystals, as seen in Fig. 1. An absorption spectrum, taken immediate after synthesis, confirms the quality of the nanocrystals (Fig. 2).

Nanocrystal solution

The electrophoretic deposition solution was produced by air drying 3 ml of as-synthesized Eu_2O_3 nanocrystal solution, yielding a nanocrystal powder. Thereafter, the powder was mixed with 20 ml of hexane (99.99% Fisher Scientific) that was either pre-chilled to –25 °C (chilled films) or kept at room temperature (room temperature films) prior to mixing. The room temperature solution was transferred to the EPD system for deposition. The resultant chilled film solution was refrigerated at –25 °C for an additional hour and, then, was transferred to the EPD system immediately prior to deposition.

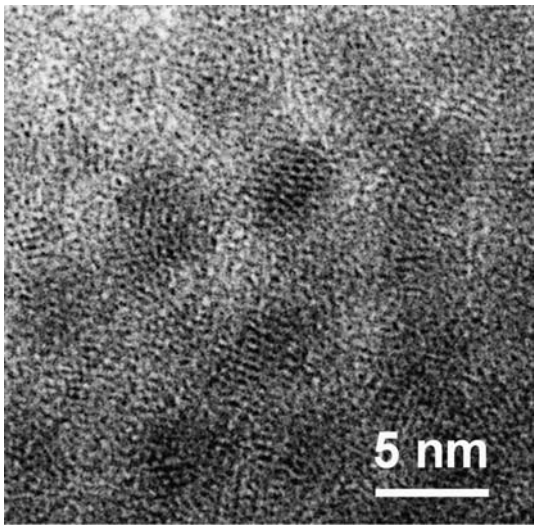

Fig. 1 Representative TEM image of the 4-nm Eu_2O_3 nanocrystals

EPD system

Figure 3 shows the schematic of the EPD apparatus used in this study. The deposition electrodes were fabricated by the thermal evaporation of approximately 20 nm of chromium and 120 nm of gold onto 2.5 cm by 1.3 cm

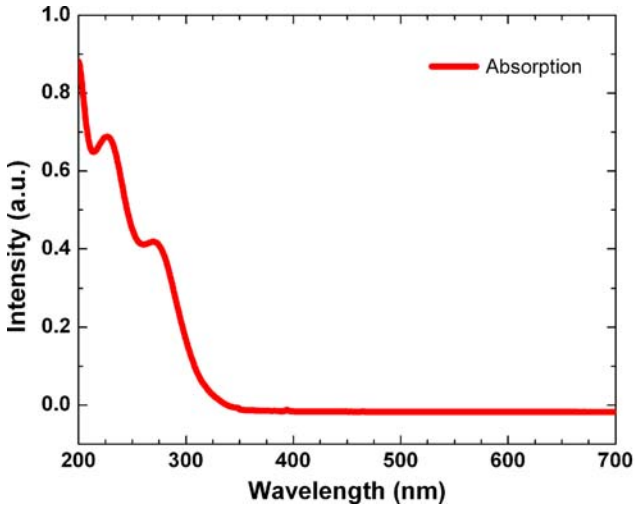

Fig. 2 Absorption spectrum of the Eu_2O_3 nanocrystals with characteristic Eu^{3+} absorption peaks at 230 nm and 270 nm

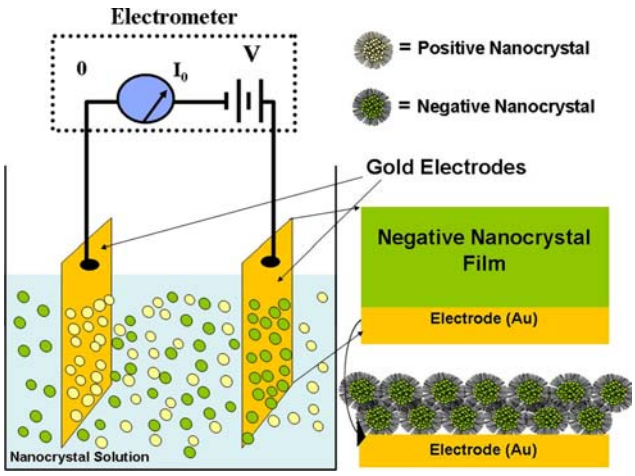

Fig. 3 Schematic of the nanocrystal electrophoretic deposition system

glass substrates. The vertically aligned electrodes were separated by approximately 2.0 mm in a parallel plate capacitor configuration. A constant applied voltage of 525 V was provided by a Keithley 6-1/2-digit Model 6517A Electrometer/High-Resistance Meter, which also measured the electrophoretic deposition current. For this study, nanocrystals were deposited during 1, 3, 7, and 10 min experiments. At the conclusion of the deposition run, the electrodes were extracted from the nanocrystal solution and were kept at 525 V for five additional minutes to anneal the film. Figure 4 illustrates a typical EPD electrode from a 10 min, chilled solution deposition.

Characterization

The crystallinity and size distribution of the nanocrystals were determined via high-resolution transmission electron microscopy (HR-TEM) using a Philips CM20T microscope, operating at 200 kV. Absorption spectra were obtained in UV–visible region using a Cary 5000 spectrophotometer. The SEM images of the films were obtained using a Hitachi S-4200 field emission scanning electron microscope, operating at 10 kV and 30 kV, coupled with an EDS detector. The optical micrographs were obtained on a Leitz Ergolux DIC photomicroscope, fitted with an Angstrom Sun CFM-USB-2 digital microscope camera.

Discussion

Analysis of scanning electron microscopy, optical microscopy, and digital photograph images of the

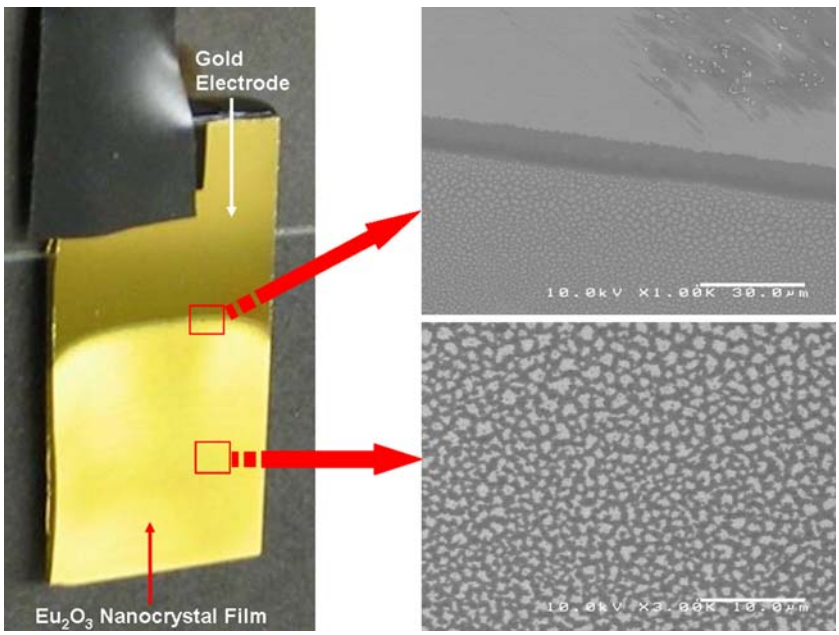

Fig. 4 Photograph of the positive electrode from a 10 min, chilled solution electrophoretic deposition experiment and SEM images of the gold–film interface and the interior of the film. Although Eu_2O_3 does not absorb strongly in the visible, Mie scattering of light off of micron-sized agglomerates provided the film a hazy, white translucent appearance. The SEM images show the interface detail between the gold and the thin film. In the SEM images, the dark gray regions correspond to the smooth, transparent, glassy films of Eu_2O_3 nanocrystals, whereas the light gray masses correspond to the micron-sized agglomerates, interspersed with the film

EPD electrodes provided insight on the film morphology and, hence, the film appearance from the different solution preparations. Figure 4 juxtaposes a photograph of an EPD electrode, from a 10 min chilled solution experiment, with its corresponding SEM images of the gold–film interface on the electrode and the interior of the film. The film's hazy, translucent appearance was attributed to Mie scattering off of micron-sized, optically transparent aggregates of nanocrystals, which appeared as light gray masses, dispersed within a dark gray background in the SEM images. For these films, the gray background corresponded to the smooth, transparent, glassy film of Eu_2O_3 nanocrystals in which the aggregates were dispersed.

Timed electrophoretic deposition experiments were conducted on both room temperature and chilled europium oxide nanocrystal solutions to investigate the relationship among the microstructure, the deposition time, and the overall appearance of the resultant nanocrystal thin films. Of the timed experiments, the 1 min deposition of the chilled film proffered most concise information about the constituents and the overall microstructure of both the room temperature and the chilled solution films. As evidenced in the SEM image of Fig. 5, three distinct materials were identified in the electrode images. The darkest regions in the image corresponded to the bare gold substrate; its chemical composition was confirmed by EDS, also seen in Fig. 5. Only gold, chromium, and silicon, which originated from the SEM detector tip, were evident in the spectrum. A second material appeared as a faint, grayish region that partially covered the electrode. This corresponded to the glassy, homogeneous Eu_2O_3 nanocrystal film that pervaded the substrate's surface. Dispersed evenly throughout the substrate also were micron-sized aggregates of Eu_2O_3 nanocrystals, seen as bright spots in the SEM image. The EDS spectra for the aggregates and the homogeneous film were identical, revealing traces of europium, sodium, and chlorine. Only the secondary X-ray lines for europium are visible within the energy range of our detector; thus, the relative intensity of the europium peak was not indicative of a paucity of Eu_2O_3 nanocrystals on the gold electrode. Further, sodium chloride (NaCl) is a byproduct of the nanocrystal synthesis, which explained its presence in the EDS spectrum.

In the subsequent experiments, we monitored the morphology, surface coverage, and distribution of these three film components, for longer EPD experiments for both room temperature and chilled solutions, through optical micrographs and SEM images (Fig. 6). For all of the image pairs, the brightly colored background of the optical micrographs, on the left,

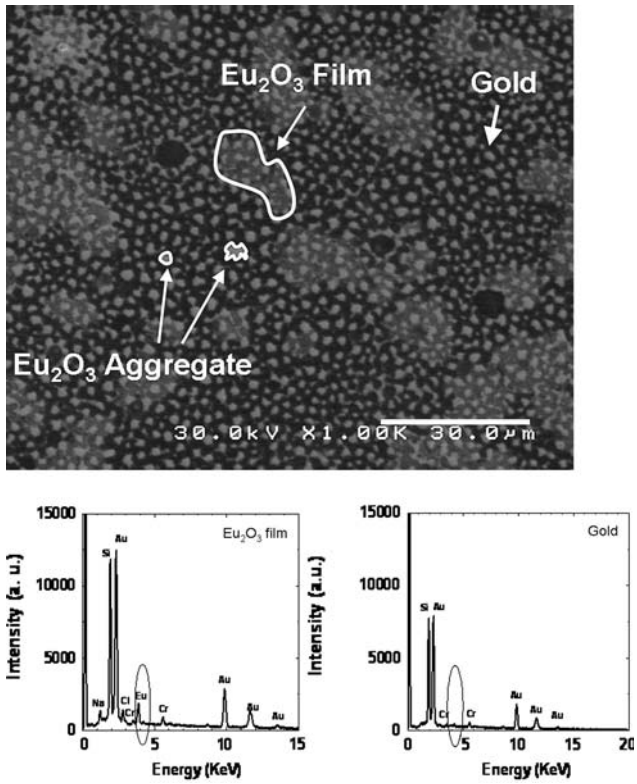

Fig. 5 SEM image of the nanocrystal film, formed during a 10 min, chilled solution electrophoretic deposition experiment. The dark background in the image represented the bare electrode. EDS on this region confirmed the presence of gold and chromium alone. Micron-size light gray spots represented the Eu_2O_3 nanocrystals agglomerates; the light gray regions correspond to the glassy Eu_2O_3 nanocrystal film. EDS taken on this region of the electrode yielded the characteristic europium signature

corresponded to the darkly shaded regions of the SEM images, on the right. As well, the very bright and very dark spots in the optical micrograph correspond to the bright spots in the SEM image. Beginning with the 1 min deposition images, both the micrograph and its complementary SEM image show the micron-sized, optically transparent aggregates amidst the transparent, glassy nanocrystal film regions, like that observed in Fig. 5. As the deposition time increased from 3 min up to 10 min, the density of the aggregates, scattered within the film, increased. For the 7 min deposition, the microstructure began to change, as clusters, large groups of aggregates, began to form within the films. (See the circled feature in the 7 min optical micrograph.) These clusters, which were not uniformly distributed throughout the film, were ascribed to electric field gradients at the electrodes near already deposited aggregates. The film prepared from the 10 min deposition experiment showed the highest density of the aggregates.

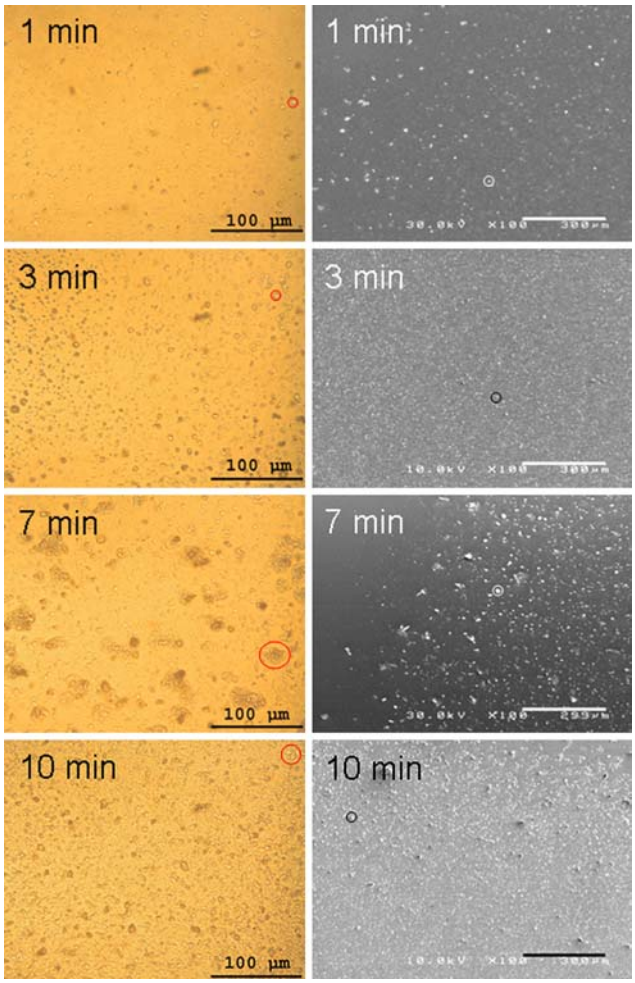

Fig. 6 Optical micrographs (left column) and SEM images (right column) of the Eu_2O_3 nanocrystal films, deposited from chilled solutions during different time durations runs. Note that the complementary SEM and optical microscope images do not correspond to exactly the same position on the sample

When we examined the 10 min EPD films from the room temperature and the –25 °C solutions, we observed a marked difference in their microstructure, as evinced in Fig. 7. The room temperature runs produced a diversity of aggregate shapes and sizes, many of which larger than 10 μm, distributed irregularly about the electrode. These misshaped, splotchy aggregates were the very dark gray regions in the SEM image. The interstitial regions, which appeared as a light gray, corresponded to the glassy nanocrystal film. These large aggregates gave the room temperature films their clouded, opaque appearance.

A plausible explanation for the temperature dependence observed in the room temperature and the chilled films can be attributed to effects on the Debye screening length (κ^{-1}) and the nanocrystal mobility, via the solution viscosity. As the solution temperature

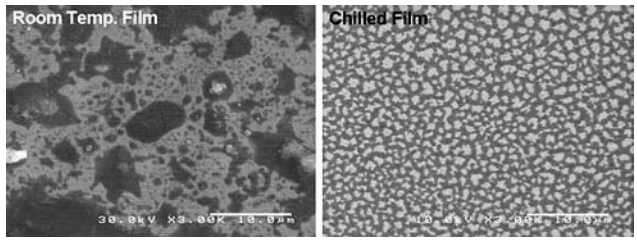

Fig. 7 SEM images of the 10 min deposition films of Eu_2O_3 nanocrystals made from (a) room temperature and (b) chilled solutions. For the room temperature image, the light gray region represented the glassy film of Eu_2O_3 nanocrystals, and dark gray areas represented the micron-sized Eu_2O_3 agglomerates. For the chilled image, the micron-size agglomerates (light gray) were uniformly dispersed within the glassy Eu_2O_3 thin film (dark gray)

decreased, both the aggregation rate and the aggregation size decreased. This was due to a decrease in the screening length ($\kappa^{-1} \propto \sqrt{\text{Temperature}}$), which then suppressed the coulombic attraction between and, hence, the aggregation of the nanocrystals [25, 26]. An increase in the viscosity of the hexane solvent and, hence, of the nanocrystal solution also was observed. Since the chilled solution was refrigerated for 1 h, the larger, irregularly shaped aggregates, normally observed at room temperature, were suppressed. This resulted in smaller agglomerates and individual nanocrystals suspended in the solution and, therefore, available for deposition onto the electrodes. Thus, the chilled nanocrystal solution, with its concentration of individual nanocrystals and smaller nanocrystal aggregates, provided a more uniformly distributed film microstructure than its room temperature counterpart.

Conclusions

Translucent and opaque thin films of 4.0 nm europium oxide nanocrystals were produced via electrophoretic deposition. Chilled (–25 °C) nanocrystal solutions yielded translucent films with more uniform microstructure than that observed for room temperature nanocrystal solutions. One minute deposition experiments with the chilled solutions provided evidence of the primary constituents of the thin films, micron-sized aggregates, and glassy, transparent nanocrystal films. Continued studies of the EPD of these nanocrystals may lead to the fabrication of wholly transparent thin films, which would be very attractive for use in electroluminescent video displays, ultraviolet-photoactive optical coatings, and other optical applications. This could be achieved by decreasing the solution temperature further or by selective filtration of the nanocrystal aggregates.

Acknowledgements The authors would like to thank Sandra Rosenthal and Dmitry Koktysh for fruitful discussions and Enrique Jackson for assistance with the optical microscopy images. This research is supported in part by Vanderbilt Institute for Nanoscale Science and Engineering (VINSE).

References

1. Leskelä M, Niinistö L (1992) Mater Chem Phys 31:7
2. Shea L, Mckittrick J, Lopez O, Sluzky E (1996) J Am Ceram Soc 79:3257
3. Meltzer RS, Hong KS (2000) Phys Rev B 61:3396
4. Ram S, Mohanty P (2002) J Mat Sci Lett 21:1127
5. Mohanty P, Ram S (2003) J Mat Chem 13:3021
6. Bazzi R, Flores MA, Louis C, Lebbou K, Zhang W, Dujardin C, Roux S, Mercier B, Ledoux G, Bernstein E, Perriat P, Tillement O (2004) Colloid Interf Sci 273:191
7. Carnall T, Fields PR, Rajnak KJ (1968) J Chem Phys 49:4450
8. Eilers H, Tissue BM (1996) Chem Phys Lett 251:74
9. Bihari B, Eilers H, Tissue BM (1997) J Lumin 75:1
10. Wakefield G, Heron HA, Dobson PJ, Hutchinson JL (1999) J Colloid Interf Sci 215:179
11. Feng J, Shan G, Maquieira A, Koivunen ME, Guo B, Hammock BD, Kennedy IM (2003) Anal Chem 75:5288
12. Härmä H, Soukka T, Lövgren T (2001) Clin Chem 47:561
13. Raue R, Vink AT, Welker T (1989) Philips Tech Rev 44:225
14. Jiao H, Wang J, Liao F, Tian S, Jing X (2004) J Electrochem Soc 151:H49
15. Mochizuki S, Nakanishi T, Suzuki Y, Ishi K (2001) Appl Phys Lett 79:3785
16. Ono H, Kusumata T (2001) Appl Phys Lett 78:1832
17. Singh MP, Shivashankar SA (2005) J Cryst Grow 276:148
18. Wong EM, Searson PC (1999) Appl Phys Lett 74:2939
19. Islam MA, Herman IP (2002) Appl Phys Lett 80:823
20. Maenosono S, Okubo T, Yamaguchi Y (2003) J Nano Res 5:5
21. Islam MA, Xia Y, Telesca Jr DA, Steigerwald ML, Herman IP (2004) Chem Mater 16:49
22. Murray CB (1995) Synthesis and characterization of II–VI quantum dots and their assembly into 3D quantum dot superlattices. Massachusetts Institute of Technology, Cambridge, MA, PhD thesis, 164pp
23. Kagan CR, Murray CB, Bawendi MG (1996) Phys Rev B 54:8633
24. Murray CB, Kagan CR, Bawendi MG (2000) Annu Rev Mater Sci 30:545
25. Gonzales-Cuenca M, Maarten Biesheuvel P, Verweij H (2000) AIChE J 46:626
26. Preston MA, Kornbrekke R, White LR (2005) Langmuir 21:9832